

**NASA
Technical
Paper
3602**

July 1996

71156

**Computational Simulation of Continuous
Fiber-Reinforced Ceramic Matrix
Composites Behavior**

Pappu L.N. Murthy,
Christos C. Chamis,
and Subodh K. Mital



National Aeronautics and
Space Administration

Trade names or manufacturers' names are used in this report for identification only. This usage does not constitute an official endorsement, either expressed or implied, by the National Aeronautics and Space Administration.

**NASA
Technical
Paper
3602**

1996

Computational Simulation of Continuous
Fiber-Reinforced Ceramic Matrix
Composites Behavior

Pappu L. N. Murthy
and Christos C. Chamis
*Lewis Research Center
Cleveland, Ohio*

Subodh K. Mital
*University of Toledo
Toledo, Ohio*



National Aeronautics and
Space Administration

Office of Management

Scientific and Technical
Information Program

Computational Simulation of Continuous Fiber-Reinforced Ceramic Matrix Composites Behavior

Pappu L. N. Murthy and Christos C. Chamis
National Aeronautics and Space Administration
Lewis Research Center
Cleveland, Ohio 44135

Subodh K. Mital
University of Toledo
Toledo, Ohio 43606

Summary

This report describes a methodology which predicts the behavior of ceramic matrix composites and has been incorporated in the computational tool CEMCAN (CEramic Matrix Composite ANalyzer). The approach combines micromechanics with a unique fiber substructuring concept. In this new concept, the conventional unit cell (the smallest representative volume element of the composite) of the micromechanics approach is modified by substructuring it into several slices and developing the micromechanics-based equations at the slice level. The methodology also takes into account nonlinear ceramic matrix composite (CMC) behavior due to temperature and the fracture initiation and progression. Important features of the approach and its effectiveness are described by using selected examples. Comparisons of predictions and limited experimental data are also provided.

Introduction

Ceramic matrix composites (CMC's) are the subject of much research because new high-temperature materials are required for structural components and other applications in high-speed engines. Continuous fiber-reinforced ceramic matrix composites are promising candidates and efforts to develop them are considerable. In comparison with conventional materials, CMC's offer several advantages: high specific stiffness and strength, higher toughness and nonbrittle failure as compared with monolithic ceramics, environmental stability, and wear resistance for both room- and elevated-temperature applications. Ceramic matrix composites are reinforced primarily to enhance toughness. A weak fiber-matrix interface allows the toughening mechanisms such as fiber bridging, crack deflection, matrix microcracking, fiber debonding, and fiber pullout to be combined to reduce residual stresses and eliminate catastrophic failures. However, the full utilization of these materials can only be achieved by their accurate micromechanical representation.

The analysis of CMC materials requires specialized modeling which considers their unique physical and mechanical behavior. Ceramic matrix composite materials are usually reinforced by high stiffness fibers, the role of which, in addition to providing higher stiffness, is to enhance toughness because the matrix material is quite brittle and fails at relatively low strain levels. In CMC's the moduli of fibers and matrix are usually of the same order. The research in CMC analytical modeling under the sponsorship of HITEMP (HIgh Temperature Engine Materials Program) at the NASA Lewis Research Center in Cleveland, Ohio, has resulted in the computational tool CEMCAN (CEramic Matrix Composite ANalyzer) which predicts CMC behavior.

The methodology incorporated in CEMCAN is based on micromechanics models in which customarily a representative volume element or unit cell is arranged in a square array pattern. However, the present approach employs a unique multilevel substructuring technique that allows the capture of greater local detail. This technique has four levels of substructuring: from laminate to ply, to subply, and then to fiber (figs. 1 and 2). The fiber is substructured into several slices and the micromechanics equations are applied at the slice level. Although the basic philosophy can be applied to the analysis of any continuous fiber-reinforced composite, the emphasis here is on the development of a computer code to specifically analyze and simulate aspects unique to ceramic matrix composites. The aspects of interest include varying degrees of interfacial bond around the fiber circumference and accounting for the fiber breaks and local matrix cracking that may lead to the rapid degradation of the interphase at higher temperatures as a result of oxidation. In addition, the multilevel substructuring technique used here can account for different fiber shapes and can integrate the effect of all of these aspects on composite properties and/or responses, in turn providing greater details about stress distribution.

The objective of this report is to describe the methodology and illustrate its effectiveness with appropriate examples, which include computing the following: composite equivalent mechanical properties; microstresses in various regions due to varying degrees of interfacial bond; nonlinear material behavior due to temperature and stress redistribution caused by

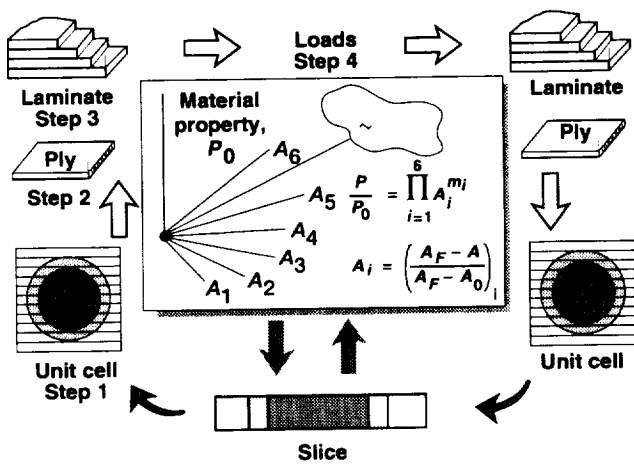
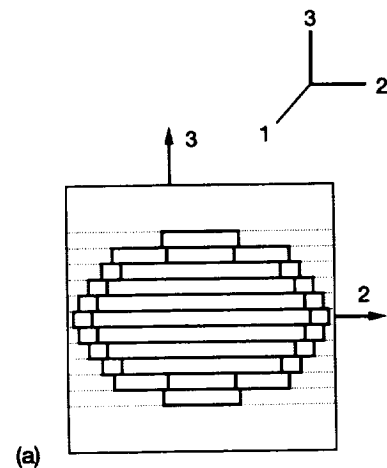


Figure 1.—Integrated analysis approach embedded in CEMCAN computer code.

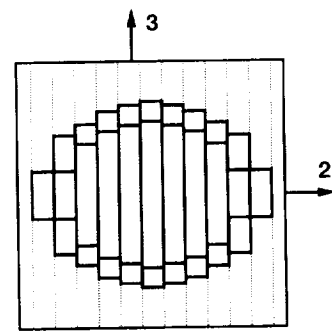
progressive fracture and/or damage under thermal and mechanical loading. The predictions made, based on the present methodology, will also be compared with experimental results. Appendix A contains a list of symbols used in this report.

Fiber Substructuring and Micromechanics

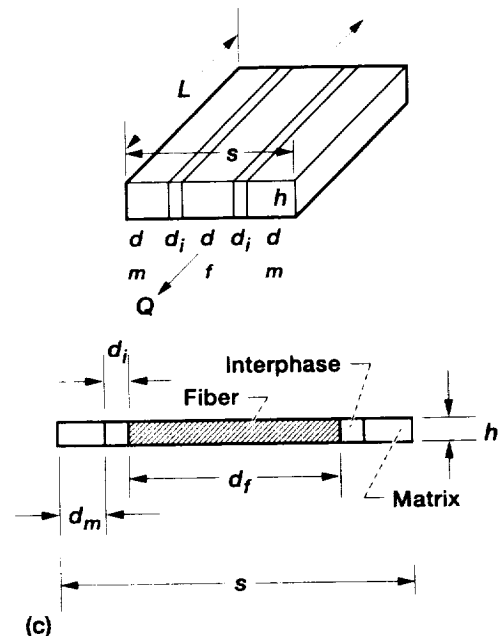
The primary objective of composite micromechanics is to determine the equivalent elastic properties of a composite material in terms of the elastic properties of the constituent materials. The properties of interest are composite moduli, Poisson's ratios, thermal expansion coefficients, thermal conductivities, heat capacity, and various composite strengths. Identifying the smallest representative unit volume element (RVE) is usually the starting point for any micromechanics approach. The micromechanics equations are derived for this element which is sometimes referred to as a "unit cell." It is the smallest region over which the stresses and strains are assumed to be macroscopically uniform. However, within the unit cell the stresses and strains are nonuniform due to the heterogeneity of the material. The unit cell consists of fiber, matrix, and possibly an interphase treated as a separate constituent. It is assumed that these cells are arranged in a regular square array pattern. Equivalent material properties for the ply are then derived in terms of constituent material properties based on the mechanics of materials approach. Other assumptions are that (1) the fiber and matrix are subjected to the same strain in the fiber direction of a unidirectional fibrous composite and (2) the same transverse stress is applied to both the fiber and matrix in the direction transverse to the fiber. These are standard assumptions for a mechanics of materials approach. However, it should be noted that such an approach is not mathematically rigorous. It only ensures the force equilibrium in all directions. A mathematically rigorous solution that ensures the continuity of strains, displacements, and stresses across the fiber and matrix



(a)



(b)



(c)

Figure 2.—Ply/fiber substructuring concepts for ceramic matrix composites micromechanics. (a) Horizontal slicing (along 2-2 direction). (b) Vertical slicing (along 3-3 direction; note: 1-1 is along fiber direction). (c) Individual slice showing fiber, matrix, and interphase regions.

boundary can be accomplished through the use of the theory of elasticity. However, the solution of elasticity equations for a composite material is quite tedious.

The present methodology for CMC's uses a unique fiber substructuring approach to derive the micromechanics equations. The unit cell is further subdivided into several slices. The equations for micromechanics are derived for slices; that is, the slice equivalent properties are computed based on the properties of the fiber, matrix, and interphase. The fiber substructuring and slice geometry are shown in figure 2. The derivation of the micromechanics equations and the assumptions involved with the approach are not given here but are documented in references 1 and 2. The equations, however, are presented in appendix B for the sake of completeness. When the equivalent slice properties are acquired, the equivalent properties of the unit cell, or RVE, are obtained by using the laminate theory in a manner analogous to obtaining laminate properties from ply properties. It should also be mentioned that 2-2, or horizontal, slicing is used to compute 1-1 and 2-2 slice properties whereas 3-3, or vertical, slicing is used to compute slice properties in the 3-3 direction.

The fiber substructuring approach is general and versatile and can be applied to any type of continuous fiber-reinforced matrix composite. Also, the fiber shape or geometry does not pose a problem at all so that various types of fiber cross sections can be routinely analyzed with the present approach. Slicing details must be provided through user subroutines for fibers that do not have a circular cross section. For circular cross sections, the program automatically does the slicing. However, analyses for other fiber shapes are beyond the scope of the present report and therefore are not examined. By carefully controlling the number of slices, one can easily incorporate various degrees of bond around the fiber circumference and along the length, fiber breaks and matrix microcracking, and effects of these parameters on ply thermal and mechanical properties and/or responses.

Material Nonlinear Behavior

At NASA Lewis over the last two decades, research to simulate the behavior of composite materials has culminated in a unified law to describe the material degradation behavior. This law, referred to as the multifactor interaction relationship (MFIR), accounts for the degradation effects of environment, fabrication, and load on constituent material behavior. In the present work, the constituent properties, namely the modulus and coefficient of thermal expansion, are considered a function of temperature only. For example the modulus is assumed to have the following functional relationship with temperature:

$$\frac{E}{E_0} = \left(\frac{T_f - T}{T_f - T_0} \right)^n \quad (1)$$

where E is the modulus at temperature T , E_0 is the reference modulus at the room temperature T_0 , and T_f is the final temperature where the modulus is zero. Based on the available experimental data, the exponent n and the final temperature T_f must be computed separately for fiber and matrix properties. Details of one such computation for the SiC/RBSN composite is given later in the section Results and Discussion.

Microstresses and Stress Redistribution Due to Progressive Fracture

The thermal and mechanical loads are specified or obtained at the laminate level. Through the successive use of lamination theory, the stresses and strains at the midplane of the plies and then at the midplane of the slices are obtained. The constituent microstresses are then computed from microstress equations that relate the equivalent slice stresses to the constituent stresses. These equations, which are based on the principles of micromechanics, are listed in appendix C.

In the stress-strain curve (in addition to any material nonlinearities mentioned above), ceramic matrix composites also show nonlinear behavior due to matrix microcracking that leads to stress redistribution as the fracture initiates and propagates. These parameters can be accounted for automatically. The microstresses are computed in all the constituents of a slice first, and the stress in each constituent is examined for failures. In the present methodology, a maximum stress-based criterion is used for the initiation of damage or fracture. However, any other failure criterion that depends on combined stresses can be easily used. Accordingly, if a constituent stress has exceeded the corresponding strength value, the constituent is assumed to have failed and the corresponding modulus of that constituent is reduced to an almost negligible value. A slice is assumed to have failed in the longitudinal direction if the fiber portion of the slice indicated a stress higher than the fiber fracture strength in the longitudinal direction. Similarly, a slice is assumed to have failed in the transverse direction if matrix region stresses indicated failure in the transverse normal or shear direction, respectively. Once a slice fails, all the microstresses that are carried by that slice up to that load step are redistributed in the slices that have not failed. The load that was carried by the failed slice is then added appropriately to the laminate load and a laminate analysis is conducted again. The load redistribution due to progressive fracture is shown schematically in figure 3. This process is continued for a given load step until an equilibrium (convergence) state is reached between the applied load and a damage state. Presently, the convergence is checked for laminate midplane strains and ply and slice strains. When all the strains are within 5 percent of the previous iteration, convergence is assumed to have been reached. This mechanism is mainly responsible for the overall nonlinear behavior in the laminate stress-strain curves at room temperature. A detailed

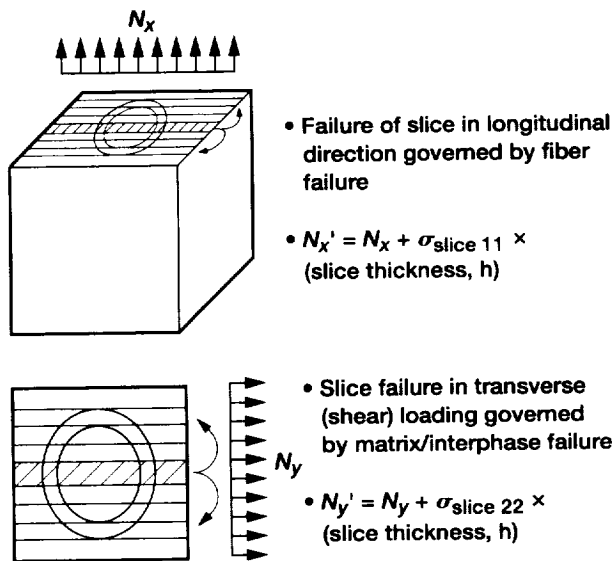


Figure 3.—Local stress redistribution due to progressive fracture. Failure based on maximum stress criterion.

description of material nonlinearities and progressive damage modeling can be found in reference 3.

CEMCAN Computer Code

The methodology just described incorporates fiber substructuring, material nonlinearities, progressive stress redistribution effects, and micro- and macromechanics equations and has been programmed into a stand-alone computer code CEMCAN. The flowchart of the program is shown in figure 1. The transition of slice properties to equivalent-unit-cell (or RVE) properties is achieved by using the classical laminate theory. If there is only one fiber through the ply thickness, the ply equivalent properties are identical to the properties of the unit cell or the RVE. If there are a number of fibers through the thickness of a single ply, the unit cell properties have to be integrated by using the classical laminate theory again to obtain the ply properties. Then, the laminate or composite properties are obtained from the single ply properties by using macromechanics theories. The classical laminate theory will not be explained here because it can be found in any composite mechanics textbook (ref. 2). After the laminate properties are computed, the next step is to obtain the laminate response due to externally applied loads. The various steps involved are depicted in figure 1. The left side of the flowchart shows the integration or synthesis of the properties from the slice (lowest) to the laminate (global) level. The right side of the flowchart shows the decomposition of the response from laminate to ply, to slices, and then to microstresses when thermal/mechanical loads are applied. The structure of the CEMCAN computer code closely resembles the previously developed composite mechanics codes at NASA Lewis (refs. 4 and 5).

Currently, the code can predict the composite mechanical and thermal properties and can compute the stresses at ply, slice, or constituent levels, thus allowing the prediction of very detailed stress gradients at a high computational efficiency. Although the results are not shown herein, the thermal and mechanical properties, as well as the microstress predictions, have been verified with other micromechanics theories and very detailed three-dimensional finite element analyses. The user can specify the number of slices in a unit cell and the state of interfacial bonding around the fiber circumference in each slice; the bonding ranges from 0 (completely debonded) to 1 (fully bonded). To obtain the mechanical properties of the interphase, the values provided in the resident data bank are multiplied by the factor (0 to 1) representing interfacial bonding. Thus, if the interphase in a slice is completely debonded, the mechanical properties of the interphase will be reduced to negligible (almost zero) values. The code can also predict the stress-strain behavior of a laminate up to failure by considering the processing conditions. Two types of nonlinearities can be handled with CEMCAN. The first type is that arising from a stress redistribution in the constituents as a result of progressive damage of the interphase, matrix, or fiber within the unit cell. If a constituent fails in a slice, it unloads and its microstresses are redistributed to the unfailed regions. Consequently, the global stress-strain behavior becomes nonlinear. The second type of nonlinearity results from the dependence of constituent properties on temperature. The residual stresses resulting from the cooldown phase of the fabrication process can be tracked with the code.

Another unique feature of the computer code is the resident data base of constituent properties, which is divided into three sections. The first, consisting of fiber properties, enables the user to include any number of different properties; however, the properties must be identified by four-character code names that can be used by the program to search the data base. The second and third sections consist of matrix and interphase properties. There is no specific limit on the number of different constituent properties one can include in the data base. The complete details of the code operation and the resident data base are discussed in the CEMCAN user's guide (ref. 6).

Results and Discussion

To demonstrate the methodology and to illustrate the various current capabilities of the CEMCAN computer code, the composite system SiC/RBSN (silicon carbide SCS-6 fibers in reaction-bonded silicon nitride matrix) was chosen because of the vast amount of readily available in-house experimental data. These data are also documented in reference 7, which forms the basis for the computed properties that are used in the present study. The computation procedure used herein is described in the next section. The use of such a procedure is mandatory for any new material system in order to arrive at a set of constituent level (fiber, matrix, and interphase) properties

that will be created in the resident data base. These properties can then be used to predict the thermomechanical response of ceramic matrix composites made of any layup type.

Prediction of Thermal and Mechanical Properties

The chosen composite system has a very compliant and weak interphase. The region between the fiber and the matrix, the interphase bonds them and is treated as a separate constituent in the study. The interphase is usually a combination of an outer carbon layer of the fiber and any reaction zone resulting from the cooldown phase of the fabrication process. The interphase properties are not readily available and therefore must be inferred from other properties. Based on photomicrographs, the interphase thickness is estimated to be approximately 3 percent of the fiber diameter ($0.03 \times 142 \mu\text{m} = 4.3 \mu\text{m}$). The nominal fiber volume ratio (fvr) for this composite was estimated to be in the range 0.3 to 0.34 in reference 7. It is well known that the interphase properties have very little effect on the longitudinal modulus of a unidirectional composite (ref. 8); therefore, we calculated the nominal fiber volume ratio to be 0.36 by comparing the measured and predicted values of longitudinal modulus for a unidirectional composite (fiber and matrix moduli are known).

For the purpose of modeling, two assumptions were made: the formation of the interphase erodes the fiber, thereby reducing its effective diameter, whereas the matrix material remains

the same. Consequently, the fiber volume ratio is reduced but the matrix volume ratio remains unchanged. For example, in the present analysis, the gross fiber volume ratio was 0.36, the fiber diameter was $142 \mu\text{m}$, and the interphase thickness was 3 percent of the fiber diameter. Effectively, then, the fiber volume ratio was reduced to 0.318, the interphase volume ratio was 0.042, and the matrix volume ratio remained unchanged at 0.64. On the other hand, if voids exist, the matrix modulus is appropriately reduced in proportion to the amount of voids internally. The user need only give the amount of voids or porosity. When the nominal fvr is known, the interphase modulus can be computed by comparing the measured and predicted values of the transverse modulus for a unidirectional composite (because the transverse composite modulus is quite sensitive to interfacial conditions). Alternatively, the measured value of the in-plane shear modulus for a unidirectional composite can also be used to compute the interphase modulus. The fiber and matrix properties and the computed interphase properties are shown in table I.

Once computed, the interphase property values can be used to predict the mechanical properties of laminates with general layups. Tables II and III show the properties predicted for three different laminates with fairly common layups: $[0_8]$, $[0_2/90_2]_s$, and $[\pm 45_2]_s$. Also shown are the experimentally obtained properties for the same laminates. There is excellent agreement in the results. It should be noted that measured values are based on several specimens and indicate some scatter. To allow for

TABLE I.—FIBER, MATRIX, AND CALIBRATED INTERPHASE PROPERTIES OF SiC/RBSN COMPOSITE SYSTEM

Constituent	Property								
	Poisson's ratio, ν	Modulus, E		Shear modulus, G		Coefficient of thermal expansion, α		Thermal conductivity, K	
			GPa	Mpsi	GPa	Mpsi	$10^{-6}/^\circ\text{C}$	$10^{-6}/^\circ\text{F}$	W/m-K
SiC (SCS-6) Fiber	0.17	390	56.6	117	17	4.1	2.3	22	12.7
RBSN Matrix	.22	110	15.95	45	6.5	2.2	1.2	5	2.9
Interphase	.22	3.5	.5	1.4	.2	2.0	1.1	2.0	1.2

TABLE II.—PREDICTED (CEMCAN) AND MEASURED ELASTIC PROPERTIES OF SiC/RBSN $[0_8]$ LAMINATE

[Unidirectional SiC/RBSN $[0_8]$ composite fiber volume ratio, 0.36^a.]

Value	Property							
	Young's modulus (longitudinal), E		Young's modulus (transverse), E_{22}		In-plane shear modulus, G_{12}		Poisson's ratio, ν_{12}	
	GPa	Mpsi	GPa	Mpsi	GPa	Mpsi		
Predicted	189	27.4	68.3	9.9	27	3.9		0.21
Measured ^b	193±7	28±1	69±3	10±0.4	31±3	4.5±0.4		.2

^aThe measured value of longitudinal modulus E_{11} for a unidirectional composite was used to compute fiber volume ratio (fvr) whereas the transverse modulus E_{22} was used to compute the interphase modulus.

^bReference 7.

TABLE III.—PREDICTED (CEMCAN) AND MEASURED ELASTIC PROPERTIES OF SiC/RBSN $[0_2/90_2]_s$ and $[\pm 45_2]_s$ LAMINATES

Laminate	Property							
	Poisson's ratio, ν_{12}	Young's modulus (longitudinal), E_{11}		Young's modulus (transverse), E_{22}		In-plane shear modulus, G_{12}		
			GPa	Mpsi	GPa	Mpsi	GPa	Mpsi
$[0_2/90_2]_s$	Predicted	0.112	129	18.7	129	18.7	27	3.9
	Measured ^a	.12	124±6	18±0.9	124±6	18±0.9	31±2	4.5±0.3
$[\pm 45_2]_s$	Predicted	0.46	78.6	11.4	78.6	11.4	58	8.4
	Measured ^a	.36	78±3	11.3±0.4	78±3	11.3±0.4	---	---

^aReference 7.

this scatter, one must systematically account for the variability or scatter in the properties of the constituent materials and perform probabilistic micro- and macromechanics analyses. Such procedures would generally yield the expected or mean values of the response (mechanical properties) as well as their distribution. Henceforth, one could put scatter bounds on the predicted values. An ongoing effort is to include a probabilistic description of the behavior in the methodology and to develop a formal computer code.

Prediction of Stress-Strain Behavior Under Uniaxial Loading

This section presents comparisons of experimental data and the prediction of composite behavior up to failure under uniaxial tensile loading at room temperature for various layups. Here one must account for the fabrication-induced thermal stresses as well as the material nonlinearities arising from the wide temperature range involved. To allow for the fabrication-induced thermal residual stresses in the composite behavior, one needs to specify the stress-free temperature from which the composite is cooled down to room temperature during the fabrication process. The composites are processed (i.e., nitridation is performed) between 1200 to 1400 °C. However, after performing several analyses, the stress-free temperature in the present simulations was assumed to be 900 °C so that the observed failure modes in these composites could be obtained. This suggests that at higher temperatures (900 to 1200 °C) some metallurgical mechanism is operative and prevents stress buildup above the assumed stress-free temperature (900 °C). Such observations have been made before with regard to other ceramic matrix composites (ref. 9). In the present simulations, the composites are cooled to room temperature (to 20 from 900 °C) prior to any loading.

The material nonlinear behavior due to temperature can be accounted for by using a simple functional relationship between the room-temperature reference properties and those at any temperature of the constituents. However, such an expression should be properly computed using available data for the matrix and the fiber material. The functional relationship

used herein was given in equation (1). Note that the maximum use temperature of these composites will be about 1200 °C and that very little degradation (max of 10 percent, Private communication with Dr. Ramakrishna Bhatt, Materials Division, NASA Lewis Research Center, Cleveland, OH, 1994.) of the constituent modulus exists, even at the maximum use temperature as compared with the reference property at room temperature. To take that into account, the exponent for the temperature dependence of the properties given in equation (1) is 0.25 for the fiber and 0.1 for the matrix; the final temperature T_f is taken as 2500 °C for the fiber and 2200 °C for the matrix material. These assumed values correspond to the observed degradation in the constituent material properties, namely the modulus and the thermal expansion coefficient for the use temperature range of these materials. Figure 4 shows the behavior of fiber and matrix moduli with respect to temperature according to equation (1).

To illustrate the procedure just described, the stress-strain behavior up to failure for unidirectional on- and off-axis specimens and two angle-ply laminates is predicted and compared with experimental stress-strain curves at room temperature.

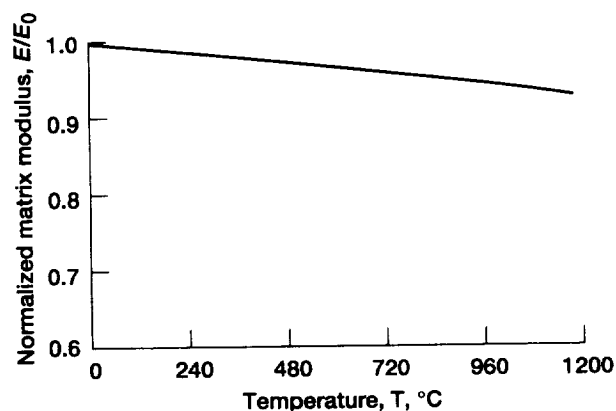


Figure 4.—Effect of temperature on constituent (fiber and matrix) moduli according to equation (1), $(E/E_0) = [(T_f - T)/(T_f - T_0)]^n$. Final fiber temperature, T_f , 2500 °C for $n = 0.25$; final matrix temperature, T_f , 2200 °C for $n = 0.1$.

The details of the simulation are shown in figures 5 to 7. The stress-strain curves for $[0]_g$ and $[90]_g$ composites are shown in figure 5. Based on the observed tensile strengths of these composites, the matrix in situ tensile strength was calibrated to

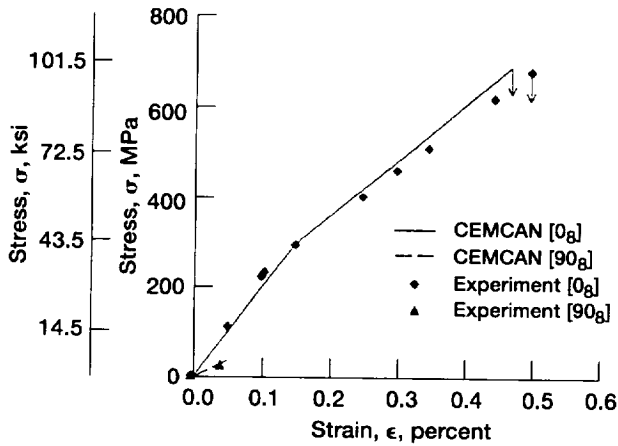


Figure 5.—Room-temperature stress-strain curves to failure of $[0]_g$ and $[90]_g$ SiC/RBSN composite.

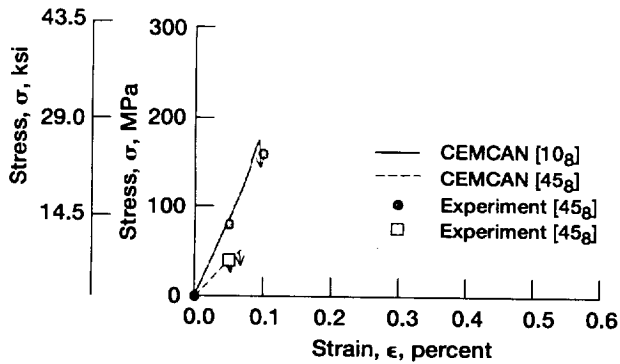


Figure 6.—Room-temperature stress-strain curves to failure of $[10]_g$ and $[45]_g$ laminates of SiC/RBSN.

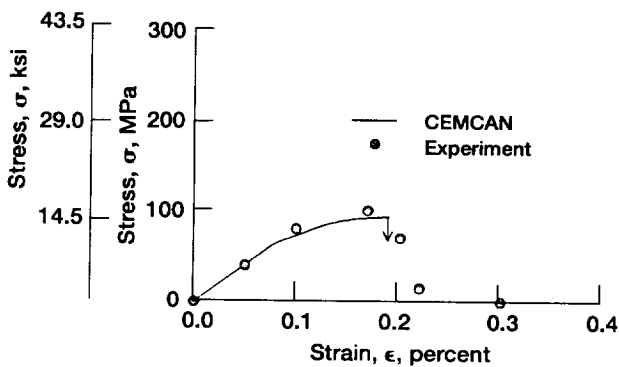


Figure 7.—Room-temperature stress-strain curves to failure of $[\pm 45]_s$ SiC/RBSN laminate.

be 100 MPa (14.5 ksi) by comparing the knee in the stress-strain curve of the $[0]_g$ composite, and the average fiber bundle strength, to be 2 GPa (285 ksi) by comparing the ultimate strength of the composite. The knee represents the initiation and subsequent saturation of the matrix microcracking. These values agree well with the fiber and matrix tensile strengths reported in reference 7. Once calibrated, the same strength values were used in subsequent simulations. The stress-strain behavior of the $[0]_g$ laminate (fig. 5) is a bilinear behavior, the knee of which represents matrix cracking to saturation. During the second part of the behavior, the load is entirely carried by fibers only. The behavior of the $[90]_g$ laminate is linear until failure, at which point the matrix failed in transverse tension at a relatively low stress level of 45 MPa (6.5 ksi).

In contrast, the off-axis laminates $[10]_g$ and $[45]_g$ stress-strain behavior is largely linear up to failure as shown in figure 6. Such behavior is characteristic of a brittle failure. The final fracture in these laminates is controlled by a combination of matrix and interphase normal and shear failure modes. The room-temperature stress-strain curve to failure for a $[\pm 45]_s$ laminate is shown in figure 7. The shear strength of the matrix is estimated to be half the matrix tensile strength to match the ultimate stress of the laminate under consideration. This laminate also fails in a combination of shear and normal failure modes and exhibits the characteristics of a graceful failure. Once again, the predicted strength of this laminate matched the experimentally measured value. Although the optical micrographs in reference 7 confirmed the aforementioned failure modes, the unloading portion of the stress-strain curve for the laminate was not predicted. The experimental data shown in these figures was taken from reference 7.

Influence of Partial Interphase Bond

The concept of fiber substructuring in the present methodology allows one to specify a partial bond around the fiber circumference and then integrate its effect up to the composite properties and response. The variation of some mechanical and thermal properties as a function of the percent of the fiber circumference debonded is shown in figure 8. Longitudinal, or fiber-controlled, properties show little degradation whereas the transverse properties reveal greater degradation as a function of debonding. Figure 9 is a comparison of composite properties normalized with respect to the value of the property for a composite with a strong interphase for a varying degree of interface bonding through the thickness. The layup is $[0]_s$ and the fiber volume ratio of the composite is 30 percent. The figure considers three levels of interfacial damage that are assumed to have taken place as a consequence of oxidation damage from exposure to high temperatures. The first case is interfacial damage only in the outer plies whereas the second case is a linearly varying degree of interfacial damage with maximum damage in the outer plies. In the third case, all the plies have the same degree of interfacial damage. The figure reveals that the

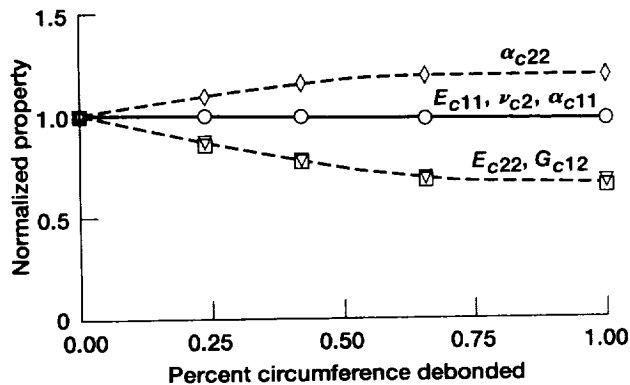


Figure 8.—Variation of thermal and mechanical properties (normalized with respect to property with strong interphase) due to partial bonding.

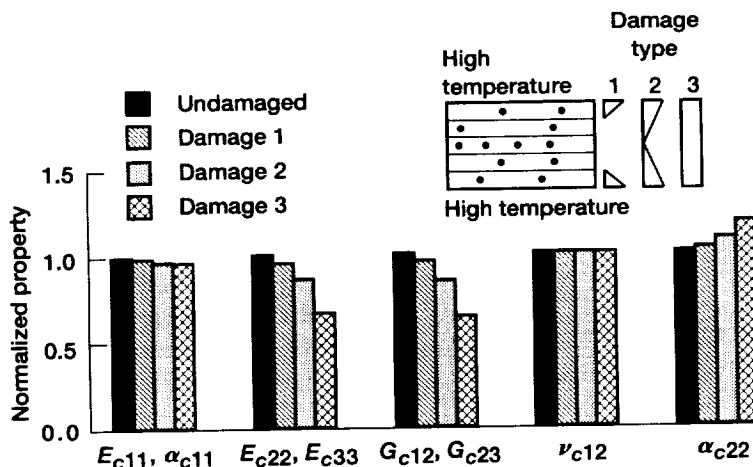


Figure 9.—Comparison of composite properties (normalized with respect to property with undamaged interphase) due to interfacial damage through the thickness; fiber volume ratio, 0.3.

damage in the interphase region leads to a varying degree of bonding and more severely effects the transverse stiffness behavior. There is a substantial reduction in the composite transverse normal and in-plane shear moduli; the longitudinal behavior is relatively unaffected.

Conclusions

A unique and novel fiber substructuring technique has been incorporated in the computer code CEMCAN to predict the behavior of ceramic matrix composites. Its features are illustrated with selected examples. Experimental validation is provided where the data are available. This concept enables one to study in great local detail ceramic matrix composite behavior pertaining to interfacial bonding of varying degrees. Based on the results shown for the SiC/RBSN composite system (silicon

carbide SCS-6 fibers in reaction-bonded silicon nitride matrix), the following specific conclusions can be drawn:

1. Fiber substructuring captures and represents greater local detail than other unit-cell-based micromechanics theories.
2. CEMCAN predictions have been verified successfully for the SiC/RBSN composite system for which experimentally obtained data are available.
3. The material nonlinear behavior model and distribution of progressive damage with stress have enabled the prediction of stress-strain behavior up to failure for different laminates. The agreement with experimentally observed behavior is excellent for the SiC/RBSN ceramic composite system.

Lewis Research Center
National Aeronautics and Space Administration
Cleveland, Ohio, April 26, 1996

Appendix A

Symbols

C heat capacity
 E Young's modulus
 G shear modulus
 K thermal conductivity
 k volume ratio
 T temperature
 α coefficient of thermal expansion
 ϵ strain
 ν Poisson's ratio

ρ density
 σ stress

Subscripts:

c composite or laminate
 f fiber
 i interphase
 ℓ slice
 m matrix

Appendix B

Micromechanics Equations

The micromechanics equations describing the relation between the constituent and the equivalent ply properties are derived for the unit cell using the mechanics of materials approach. The complete details can be found in reference 1. Only a brief description of the equations is given here for the sake of completeness. The modeling details for the substructured unit cell and the slice are shown in figure 2.

Equivalent Slice Properties

To derive the equivalent slice properties, consider a slice taken from the unit cell. Let d_f , d_m , and d_i be the fiber, matrix, and interphase widths and h and s be the height of the slice and the total width of the slice, respectively. Because it is customary to express the equivalent properties in terms of the properties of each constituent and its respective volume ratio, let k_f , k_m , and k_i be the fiber, matrix, and interphase volume ratios, respectively. Then, by definition,

$$k_f = \frac{d_f}{s}; k_m = \frac{2d_m}{s}; k_i = \frac{2d_i}{s} \quad (\text{B1})$$

Now that the preliminary parameters have been established, the mechanics of materials approach is applied to generate the composite mechanical and thermal properties.

Mechanical Properties

By applying the force equilibrium in the longitudinal direction, the following equation can be written:

$$\sigma_{\ell 11} h s = (2\sigma_{m 11} d_m + 2\sigma_{i 11} d_i + \sigma_{f 11} d_f) h \quad (\text{B2})$$

Also, based on the assumptions for the mechanics of materials approach, the following equation can be written as

$$\epsilon_{\ell 11} = \epsilon_{m 11} = \epsilon_{i 11} = \epsilon_{f 11} \quad (\text{B3})$$

With the aid of equations (B1) to (B3), the longitudinal modulus $E_{\ell 11}$ can be written as

$$E_{\ell 11} = k_f E_{f 11} = k_m E_{m 11} = k_i E_{i 11} \quad (\text{B4})$$

The Poisson's ratio ν in the 1-2 direction can be derived by considering the strain in the transverse direction 2-2 as the sum of the individual strains in the constituents. Accordingly,

$$\epsilon_{\ell 22} s = 2\epsilon_{m 22} d_m + 2\epsilon_{i 22} d_i + \epsilon_{f 22} d_f \quad (\text{B5})$$

Also, by definition

$$\nu_{j 12} = \frac{\epsilon_{j 22}}{\epsilon_{j 11}} \quad (\text{B6})$$

where j can represent any of the subscripts ℓ , m , or f .

The combination of equations (B1), (B5), and (B6) leads to the following equation for the major Poisson's ratio:

$$\nu_{\ell 12} = k_f \nu_{f 12} + k_m \nu_{m 12} + k_i \nu_{i 12} \quad (\text{B7})$$

The modulus in the transverse 2-2 direction can be derived by assuming that the same transverse stress $\sigma_{\ell 22}$ is applied to the fiber, matrix, and interphase:

$$\sigma_{\ell 22} = \sigma_{m 22} = \sigma_{i 22} = \sigma_{f 22} \quad (\text{B8})$$

With the aid of equations (5) and (8) and noting that one can derive the following equation for the transverse modulus in the 2-2 direction

$$\epsilon_{j 22} = \frac{\sigma_{j 22}}{E_{j 22}} \quad (\text{B9})$$

$$E_{\ell 22} = \frac{E_{m 22} E_{i 22} E_{f 22}}{k_m E_{i 22} E_{f 22} + k_i E_{f 22} E_{m 22} + k_f E_{m 22} E_{i 22}} \quad (\text{B10})$$

The in-plane shear modulus in the 1-2 direction is determined by assuming that the shearing stresses on the fiber and the matrix are the same. In this respect, the derivation of $G_{\ell 12}$ is similar to that for $E_{\ell 22}$. The equation for $G_{\ell 12}$ is

$$G_{\ell 12} = \frac{G_{m 12} G_{i 12} G_{f 12}}{k_m G_{i 12} G_{f 12} + k_i G_{f 12} G_{m 12} + k_f G_{m 12} G_{i 12}} \quad (\text{B11})$$

The remaining mechanical properties can be derived in a similar fashion and are given by

$$E_{\ell 33} = \frac{E_{m 33} E_{i 33} E_{f 33}}{k_m E_{i 33} E_{f 33} + k_i E_{f 33} E_{m 33} + k_f E_{m 33} E_{i 33}} \quad (\text{B12})$$

$$G_{\ell 33} = \frac{G_{m 13} G_{i 13} G_{f 13}}{k_m G_{i 13} G_{f 13} + k_i G_{f 13} G_{m 13} + k_f G_{m 13} G_{i 13}} \quad (\text{B13})$$

$$G_{\ell 13} = \frac{G_{m23}G_{i23}G_{f23}}{k_m G_{i23}G_{f23} + k_i G_{f23}G_{m23} + k_f G_{m23}G_{i23}} \quad (\text{B14})$$

$$v_{\ell 13} = k_f v_{f13} + k_m v_{m13} + k_i v_{i13} \quad (\text{B15})$$

$$v_{\ell 32} = k_f v_{f32} + k_m v_{m32} + k_i v_{i32} \quad (\text{B16})$$

The Poisson's ratios in the 2-3, 2-1, and 3-1 directions are given by the reciprocity relations

$$v_{\ell 23} = \frac{v_{\ell 32}E_{\ell 22}}{E_{\ell 33}} \quad (\text{B17})$$

$$v_{\ell 21} = \frac{v_{\ell 12}E_{\ell 22}}{E_{\ell 11}} \quad (\text{B18})$$

$$v_{\ell 31} = \frac{v_{\ell 13}E_{\ell 33}}{E_{\ell 11}} \quad (\text{B19})$$

Thermal Properties

The equivalent thermal conductivity in the 1-1 direction can be derived by equating the total heat flow rate across the cross section to the sum of the individual rates in each constituent. The heat flow rate can be calculated using the Fourier's law of heat conduction. By following the previous steps, the heat-flow-rate equilibrium equation can be written as

$$K_{\ell 11}sh \frac{dT}{dL} = k_{f11}d_f h \frac{dT}{dL} + K_{m11}d_m h \frac{dT}{dL} + K_{i11}d_i h \frac{dT}{dL} \quad (\text{B20})$$

where K is the thermal conductivity and (dT/dL) is the thermal gradient across a typical length of the cell L in the 1-1 direction (fig. 10). Simplification of equation (B20) leads to the following:

$$K_{i11} = k_f K_{f11} + k_m K_{m11} + k_i K_{i11} \quad (\text{B21})$$

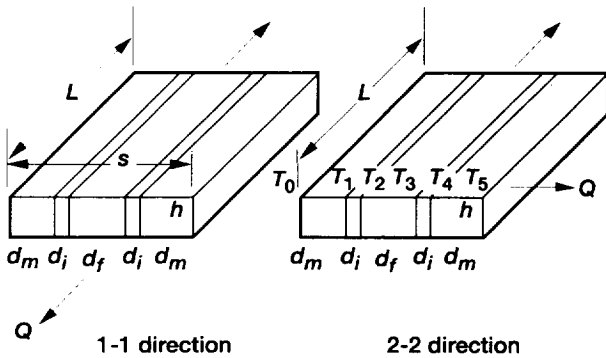


Figure 10.—Modeling details of slice for deriving equivalent slice thermal conductivities.

The equivalent thermal conductivities in the 2-2 direction can be derived by noting that the total heat flow rate across each constituent in the 2-2 direction should be the same. Thus, figure 10 shows that T_0 through T_5 are the temperatures at various cross sections along the slice. Equation (B21) can be rearranged as

$$\begin{aligned} Q &= K_{\ell 22}(Lh) \left[\frac{T_5 - T_0}{s} \right] = K_{m22}(Lh) \left[\frac{T_5 - T_4}{d_m} \right] \\ &= K_{i22}(Lh) \left[\frac{T_4 - T_3}{d_i} \right] = K_{f22}(Lh) \left[\frac{T_3 - T_2}{d_f} \right] \\ &= K_{i22}(Lh) \left[\frac{T_2 - T_1}{d_i} \right] = K_{m22}(Lh) \left[\frac{T_1 - T_0}{d_m} \right] \end{aligned} \quad (\text{B22})$$

$$\begin{aligned} K_{\ell 22} &= K_{m22} \left[\frac{T_5 - T_4}{T_5 - T_0} \right] \frac{s}{d_m} \\ &= \left[\frac{T_5 - T_4}{(T_5 - T_4) + (T_4 - T_3) + (T_3 - T_2) + (T_2 - T_1) + (T_1 - T_0)} \right] \frac{s}{d_m} \end{aligned} \quad (\text{B23})$$

By observing that $(T_4 - T_3) = (T_2 - T_1)$ and that $(T_5 - T_4) = (T_1 - T_0)$, equation (B23) can be further simplified to

$$K_{\ell 22} = \frac{1}{2 + 2 \left(\frac{T_4 - T_3}{T_5 - T_4} \right) + \left(\frac{T_3 - T_2}{T_5 - T_4} \right)} K_{m22} \frac{s}{d_m} \quad (\text{B24})$$

With the aid of equations (B1) and (B22), equation (B24) can be written as

$$K_{\ell 22} = \frac{K_{m22}}{k_m + \frac{k_i K_{m22}}{K_{i22}} + \frac{k_f K_{m22}}{K_{f22}}}$$

which leads to

$$K_{\ell 22} = \frac{K_{m22}K_{i22}K_{f22}}{k_m K_{i22}K_{f22} + k_i K_{f22}K_{m22} + k_f K_{m22}K_{i22}} \quad (\text{B25})$$

The thermal conductivity along the 3-3 direction can be derived in a similar manner and is given by

$$K_{\ell 33} = \frac{K_{m33}K_{i33}K_{f33}}{k_m K_{i33}K_{f33} + k_i K_{f33}K_{m33} + k_f K_{m33}K_{i33}} \quad (\text{B26})$$

The equivalent heat capacity C_ℓ can be derived by equating the sum of the heat contained in the individual regions to the heat contained in the slice based on the equivalent heat capacity:

$$C_\ell = \frac{k_m \rho_m C_m + k_i \rho_i C_i + k_f \rho_f C_f}{\rho_\ell} \quad (\text{B27})$$

where ρ_ℓ is the equivalent density of the slice and ρ_m , ρ_i , and ρ_f are respectively the densities of the matrix, interphase, and fiber. The equivalent density can be expressed in terms of the individual densities by the simple rule of mixtures:

$$\rho_\ell = k_f \rho_f + k_m \rho_m + k_i \rho_i \quad (\text{B28})$$

The longitudinal thermal expansion coefficient $\alpha_{\ell 11}$ can be derived by noting that the sum of the forces in the longitudinal direction should be zero:

$$\begin{aligned} & (2d_m E_{m11} + 2d_i E_{i11} + d_f E_{f11}) \alpha_{\ell 11} \Delta T \\ & = - (2d_m \alpha_{m11} E_{m11} + 2d_i \alpha_{i11} E_{i11} + d_f \alpha_{f11} E_{f11}) \Delta T = 0 \end{aligned} \quad (\text{B29})$$

where ΔT is the temperature difference. Simplification of equation (B29) leads to the following expression for the longitudinal thermal expansion coefficient:

$$\alpha_{\ell 11} = \frac{k_m \alpha_{m11} E_{m11} + k_i \alpha_{i11} E_{i11} + k_f \alpha_{f11} E_{f11}}{E_{\ell 11}} \quad (\text{B30})$$

The transverse thermal expansion coefficient can be derived by equating the total strain in the 2-2 direction to the sum of the individual strains in each region:

$$\alpha_{\ell 22} s \Delta T = 2d_m \alpha_{m22} \Delta T + 2d_i \alpha_{i22} \Delta T + d_f \alpha_{f22} \Delta T \quad (\text{B31})$$

With the aid of equations (B1) and (B31), $\alpha_{\ell 22}$ can be written as

$$\alpha_{\ell 22} = k_f \alpha_{f22} + k_m \alpha_{m22} + k_i \alpha_{i22} \quad (\text{B32})$$

The expression for $\alpha_{\ell 33}$ is similar to equation (B32) and is given by

$$\alpha_{\ell 33} = k_f \alpha_{f33} + k_m \alpha_{m33} + k_i \alpha_{i33} \quad (\text{B33})$$

This set of equations defines the equivalent properties for a typical slice with three regions. The procedure to obtain the equivalent properties of the representative volume element (unit cell) is analogous to that of obtaining the properties of a typical laminate from the ply properties. Here, each slice is treated as a subply within the unit cell.

Appendix C

Equations for Microstresses in Slice Regions

Microstresses Due To Applied Mechanical Loads

Following are the microstress equations due to applied mechanical and thermal loading.

Matrix Microstresses Due To Applied Slice Normal Stresses

$$\sigma_{m11}^{(1)} = \left(\frac{E_{m11}}{E_{\ell11}} \right) \sigma_{\ell11}$$

$$\sigma_{m11}^{(2)} = -(\nu_{\ell21} - \nu_{m21}) \frac{\sigma_{\ell22}}{E_{\ell22}} E_{m11}$$

$$\sigma_{m11}^{(3)} = -(\nu_{\ell31} - \nu_{m31}) \frac{\sigma_{\ell33}}{E_{\ell33}} E_{m11}$$

$$\sigma_{m11} = \sigma_{m11}^{(1)} + \sigma_{m11}^{(2)} + \sigma_{m11}^{(3)}$$

and

$$\sigma_{m22}^{(2)} = \sigma_{\ell22}$$

$$\sigma_{m22}^{(1)} = 0$$

$$\sigma_{m22}^{(3)} = 0$$

The case for 3-3 is the same; just replace 2-2 with 3-3.

Interphase Microstresses Due To Applied Slice Normal Stresses

$$\sigma_{i11}^{(1)} = \left(\frac{E_{i11}}{E_{\ell11}} \right) \sigma_{\ell11}$$

$$\sigma_{i11}^{(2)} = -(\nu_{\ell21} - \nu_{i21}) \frac{\sigma_{\ell22}}{E_{\ell22}} E_{i11}$$

$$\sigma_{i11}^{(3)} = -(\nu_{\ell31} - \nu_{i31}) \frac{\sigma_{\ell33}}{E_{\ell33}} E_{i11}$$

$$\sigma_{i11} = \sigma_{i11}^{(1)} + \sigma_{i11}^{(2)} + \sigma_{i11}^{(3)}$$

and

$$\sigma_{i22}^{(2)} = \sigma_{\ell22}$$

$$\sigma_{i22}^{(1)} = 0$$

$$\sigma_{i22}^{(3)} = 0$$

The case for 3-3 is the same; just replace 2-2 with 3-3.

Fiber Microstresses Due To Applied Slice Normal Stresses

$$\sigma_{f11}^{(1)} = \left(\frac{E_{f11}}{E_{\ell11}} \right) \sigma_{\ell11}$$

Poisson's effect is computed from equilibrium considerations:

$$k_f \sigma_{f11}^{(2)} + k_m \sigma_{m11}^{(2)} + k_i \sigma_{i11}^{(2)} = 0$$

Microstresses Due To Applied Slice Shear Stresses

$$\sigma_{f12} = \sigma_{i12} = \sigma_{m12} = \sigma_{\ell12}$$

$$\sigma_{f13} = \sigma_{i13} = \sigma_{m13} = \sigma_{\ell13}$$

$$\sigma_{f23} = \sigma_{i23} = \sigma_{m23} = \sigma_{\ell23}$$

Microstrains

$$\epsilon_{f12} = \frac{\sigma_{f12}}{G_{f12}}; \quad \epsilon_{i12} = \frac{\sigma_{i12}}{G_{i12}}; \quad \epsilon_{m12} = \frac{\sigma_{m12}}{G_{m12}}, \quad \text{etc.}$$

Microstresses Due To Applied Thermal Loads

Matrix Microstresses

$$\sigma_{m11} = (\alpha_{\ell 11} - \alpha_{m11})\Delta TE_{m11}$$

$$\sigma_{m22} = (\alpha_{\text{ply } 22} - \alpha_{\ell 22})\Delta TE_{m22}$$

Interphase Microstresses

$$\sigma_{i11} = (\alpha_{\ell 11} - \alpha_{i11})\Delta TE_{i11}$$

$$\sigma_{i22} = (\alpha_{\text{ply } 22} - \alpha_{\ell 22})\Delta TE_{i22}$$

Fiber Microstresses

$$\sigma_{f11} = (\alpha_{\ell 11} - \alpha_{f11})\Delta TE_{f11}$$

$$\sigma_{f22} = (\alpha_{\text{ply } 22} - \alpha_{\ell 22})\Delta TE_{f22}$$

Note: Restrained stresses/strains will be generated for the unit cell through the lamination theory application to the substructured fiber.

References

1. Murthy, P.L.N.; and Chamis, C.C.: Towards the Development of Micromechanics Equations for Ceramic Matrix Composites via Fiber Substructuring. NASA TM-105246, 1992.
2. Agarwal B.D.; and Broutman, L.J.: Analysis and Performance of Fiber Composites. Second ed., Wiley & Sons, New York, 1990.
3. Mital, S.K.; Murthy, P.L.N.; and Chamis, C.C.: Modeling of Stress/Strain Behavior of Fiber-Reinforced Ceramic Matrix Composites Including Stress Redistribution. NASA TM-106789, 1994.
4. Murthy, P.L.N.; Ginty, C.A.; and Sanfeliz, J.G.: Second Generation Integrated Composite Analyzer (ICAN) Computer Code. NASA TP-3290, 1993.
5. Lee, H.-J. et al.: Metal Matrix Composite Analyzer (METCAN) User's Manual-Version 4.0. NASA TM-105244, 1992.
6. Mital, S.K.; and Murthy, P.L.N.: CEMCAN-Ceramic Matrix Composites Analyzer User's Guide-Version 2.0. NASA TM-107187, 1996.
7. Bhatt, R.T.; and Phillips, R.E.: Laminate Behavior for SiC Fiber-Reinforced Reaction-Bonded Silicon Nitride Matrix Composites. NASA TM-101350, 1988.
8. Mital, S.K.; Murthy, P.L.N.; and Chamis, C.C.: Ceramic Matrix Composites Properties/Microstresses With Complete and Partial Interphase Bond. NASA TM-106136, 1993.
9. Rousseau, C.Q.; Davidson, D.L.; and Campbell, J.B.: Micromechanics of Ambient Temperature Cyclic Fatigue Loading in a Composite of CAS Glass Ceramic Reinforced With Nicalon Fibers. J. Compos. Technol. Res., vol. 16, no. 2, April 1994, pp. 115-126.

REPORT DOCUMENTATION PAGEForm Approved
OMB No. 0704-0188

Public reporting burden for this collection of information is estimated to average 1 hour per response, including the time for reviewing instructions, searching existing data sources, gathering and maintaining the data needed, and completing and reviewing the collection of information. Send comments regarding this burden estimate or any other aspect of this collection of information, including suggestions for reducing this burden, to Washington Headquarters Services, Directorate for Information Operations and Reports, 1215 Jefferson Davis Highway, Suite 1204, Arlington, VA 22202-4302, and to the Office of Management and Budget, Paperwork Reduction Project (0704-0188), Washington, DC 20503.

1. AGENCY USE ONLY (Leave blank)		2. REPORT DATE July 1996	3. REPORT TYPE AND DATES COVERED Technical Paper	
4. TITLE AND SUBTITLE Computational Simulation of Continuous Fiber-Reinforced Ceramic Matrix Composites Behavior			5. FUNDING NUMBERS WU-505-63-12	
6. AUTHOR(S) Pappu L. N. Murthy, Christos C. Chamis, and Subodh K. Mital				
7. PERFORMING ORGANIZATION NAME(S) AND ADDRESS(ES) National Aeronautics and Space Administration Lewis Research Center Cleveland, Ohio 44135-3191			8. PERFORMING ORGANIZATION REPORT NUMBER E-10140	
9. SPONSORING/MONITORING AGENCY NAME(S) AND ADDRESS(ES) National Aeronautics and Space Administration Washington, D.C. 20546-0001			10. SPONSORING/MONITORING AGENCY REPORT NUMBER NASA TP-3602	
11. SUPPLEMENTARY NOTES Pappu L. N. Murthy, and Christos C. Chamis, NASA Lewis Research Center; Subodh K. Mital, University of Toledo, Toledo, Ohio 43606. Responsible person, Pappu L.N. Murthy, organization code 5220, (216) 433-3332.				
12a. DISTRIBUTION/AVAILABILITY STATEMENT Unclassified - Unlimited Subject Category 24 This publication is available from the NASA Center for Aerospace Information, (301) 621-0390.			12b. DISTRIBUTION CODE	
13. ABSTRACT (Maximum 200 words) This report describes a methodology which predicts the behavior of ceramic matrix composites and has been incorporated in the computational tool CEMCAN (CEramic Matrix Composite ANalyzer). The approach combines micromechanics with a unique fiber substructuring concept. In this new concept, the conventional unit cell (the smallest representative volume element of the composite) of the micromechanics approach is modified by substructuring it into several slices and developing the micromechanics-based equations at the slice level. The methodology also takes into account nonlinear ceramic matrix composite (CMC) behavior due to temperature and the fracture initiation and progression. Important features of the approach and its effectiveness are described by using selected examples. Comparisons of predictions and limited experimental data are also provided.				
14. SUBJECT TERMS Ceramic matrix composite; Micromechanics; Progressive fracture; Unit cell; Fiber substructuring; Interphase; Interface; Progressive debonding; Partial interphase bond; Stress redistribution			15. NUMBER OF PAGES 18	
			16. PRICE CODE A03	
17. SECURITY CLASSIFICATION OF REPORT Unclassified	18. SECURITY CLASSIFICATION OF THIS PAGE Unclassified	19. SECURITY CLASSIFICATION OF ABSTRACT Unclassified	20. LIMITATION OF ABSTRACT	